Spin-orbit-coupled Bose-Einstein condensates held under a toroidal trap

Xiao-Fei Zhang,[1,2,3] Masaya Kato,[1] Wei Han,[2] Shou-Gang Zhang,[2,3,*] and Hiroki Saito[1,†]
[1]*Department of Engineering Science, University of Electro-Communications, Tokyo 182-8585, Japan*
[2]*Key Laboratory of Time and Frequency Primary Standards, National Time Service Center, Chinese Academy of Sciences, Xi'an 710600, China*
[3]*University of Chinese Academy of Sciences, Beijing 100049, China*
(Received 29 October 2016; published 16 March 2017)

We study a quasispin-1/2 Bose-Einstein condensate with synthetically generated spin-orbit coupling in a toroidal trap and show that the system has a rich variety of ground states. As the central hole region increases, i.e., the potential changes from harmoniclike to ringlike, the condensate exhibits a variety of structures, such as a modified stripe, an alternately arranged stripe, and countercircling states. In the limit of a quasi-one-dimensional ring, the quantum many-body ground state is obtained, which is found to be the fragmented condensate.

DOI: 10.1103/PhysRevA.95.033620

I. INTRODUCTION

The engineering of a synthetic gauge field and spin-orbit coupling (SOC) in neutral atomic gases recently has attracted major attention both theoretically and experimentally [1–10]. In condensed-matter physics, the SOC plays an important role for the emergence of many exotic quantum phenomena [11,12]. The creation of SOC in spinor Bose-Einstein condensates (BECs) not only offers us a new platform to simulate the response of charged particles to an external electromagnetic field, but also opens up an entirely new paradigm for studying strong correlations of quantum many-body systems, which enables quantum simulations of condensed-matter phenomena because of the high controllability of the system [13–16]. Very recently, another type of SOC, namely, the spin and orbital-angular-momentum coupling, has also been proposed [17–19].

For a homogeneous SO-coupled condensate, the mean-field ground state favors either a plane wave or a striped wave depending on the ratio between inter- and intracomponent interactions [20,21]. The presence of the trapping potential modifies this situation and leads to a rich ground-state physics [22–28]. In the presence of a two-dimensional (2D) harmonic trap, a complex phase diagram of Rashba SO-coupled Bose gases was observed in which there are two classes of phases and several subphases [23]. In addition, SO-coupled BECs subject to rotation have been studied, which exhibit a rich variety of the ground-state phases and vortex configurations depending on the strength of the SOC and rotation frequency [29–33].

Bosonic gases loaded in a toroidal trap have attracted considerable interest [34–40] where such a trapping potential can be realized by a blue-detuned laser beam to make a repulsive potential barrier in the middle of a harmonic magnetic trap [41]. The toroidal trap provides us an ideal platform to study fascinating properties of a superfluid, such as persistent flow [42–44] and symmetry-breaking localization [45,46]. Now the point is that, in the presence of a toroidal trap, we are inquisitive about whether such a potential can essentially change the properties of a SO-coupled BEC, which is what we attempt to do in this paper.

The paper is organized as follows. In Sec. II we formulate the theoretical model describing the SO-coupled BECs held under a toroidal trap. Various ground states generated by the effects of the SOC and toroidal potential are investigated using the mean-field theory in Sec. III. The quantum many-body ground state is studied in the limit of a quasi-one-dimensional (quasi-1D) ring in Sec. IV. The main results of the paper are summarized in Sec. V.

II. MODEL

We consider a two-component BEC with a Rashba SOC confined in a quasi-2D toroidal trap on the x-y plane. The second-quantized Hamiltonian of the system is given by $\hat{\mathcal{H}} = \hat{\mathcal{H}}_0 + \hat{\mathcal{H}}_{\rm int}$, where

$$\hat{\mathcal{H}}_0 = \int d\mathbf{r}\, \hat{\boldsymbol{\psi}}^\dagger \left[-\frac{\hbar^2\nabla^2}{2M} + \mathcal{V}_{\rm so} + V(r) \right] \hat{\boldsymbol{\psi}},$$
$$\hat{\mathcal{H}}_{\rm int} = \int d\mathbf{r} \left(\frac{g_{\uparrow\uparrow}}{2}\hat{\psi}_\uparrow^{\dagger 2}\hat{\psi}_\uparrow^2 + \frac{g_{\downarrow\downarrow}}{2}\hat{\psi}_\downarrow^{\dagger 2}\hat{\psi}_\downarrow^2 + g_{\uparrow\downarrow}\hat{\psi}_\uparrow^\dagger\hat{\psi}_\downarrow^\dagger\hat{\psi}_\downarrow\hat{\psi}_\uparrow \right), \tag{1}$$

where $\hat{\boldsymbol{\psi}} = (\hat{\psi}_\uparrow, \hat{\psi}_\downarrow)^T$ denotes the field operator of the atom with pseudospin state $\uparrow, \downarrow$ and M is the atomic mass. The Rashba SOC is $\mathcal{V}_{\rm so} = -i\kappa(\sigma_x\partial_x + \sigma_y\partial_y)$ with $\sigma_{x,y}$ being the Pauli matrices and κ is the strength of the SOC. Here we further assume that the two intracomponent interaction parameters are the same $g_{\uparrow\uparrow} = g_{\downarrow\downarrow} \equiv g$. When the quasi-2D system is realized by a tight harmonic potential with frequency ω_z, the effective interaction parameters are given by $g = \sqrt{8\pi}\hbar^2 a/(Ma_z)$ and $g_{\uparrow\downarrow} = \sqrt{8\pi}\hbar^2 a_{\uparrow\downarrow}/(Ma_z)$, where a and $a_{\uparrow\downarrow}$ are the corresponding s-wave scattering lengths and $a_z = \sqrt{\hbar/(M\omega_z)}$.

The trapping potential considered here is a toroidal trap, which reads

$$V(r) = \tfrac{1}{2}M\omega_\perp^2 r^2 + V_0 e^{-2r^2/\sigma_0^2}, \tag{2}$$

where $\omega_\perp$ is the radial trap frequency of the harmonic potential $r^2 = x^2 + y^2$ and V_0 and σ_0 are proportional to the intensity and beam waist of the optical plug. The bottom of the potential

*szhang@ntsc.ac.cn
†hiroki.saito@uec.ac.jp

in Eq. (2) is located at

$$R = \frac{\sigma_0}{\sqrt{2}}\sqrt{\ln\frac{4V_0}{M\omega_\perp^2\sigma_0^2}}. \tag{3}$$

Expanding Eq. (2) around $r = R$ and neglecting the third and higher orders of $r - R$, we obtain

$$V_r(r) = \frac{M\omega_0^2}{2}(r - R)^2, \tag{4}$$

where $\omega_0 = 2\omega_\perp R/\sigma_0$ and a constant is omitted. This approximation is valid when $\hbar\omega_0$ is much larger than the characteristic energy of the system.

III. MEAN-FIELD ANALYSIS

A. Ground states

We implement the mean-field approximation by replacing the field-operators $\hat{\psi}_{\uparrow,\downarrow}$ with the macroscopic wave-functions $\psi_{\uparrow,\downarrow}$ in Eq. (1), which gives the Gross-Pitaevskii (GP) energy functional. We numerically minimize it by using the imaginary time-evolution method and obtain the ground-state wave function. We work in dimensionless units by scaling with the appropriate factors of the harmonic trap energy $\hbar\omega_\perp$ and the harmonic trap length $\sqrt{\hbar/(M\omega_\perp)}$. The trapping potential in Eq. (2) can be rewritten as $V_r(r) = r^2/2 + Ae^{-r^2/l^2}$ with $l = \sqrt{M\omega_\perp\sigma_0^2/(2\hbar)}$ and $A = V_0/(\hbar\omega_\perp)$. The trapping potential in Eq. (4) is $V(r) = \tilde{\omega}_0^2(r - R)^2/2$ with $\tilde{\omega}_0 = \omega_0/\omega_\perp$.

Figure 1 shows the ground-state density profiles of the system for $g < g_{\uparrow\downarrow}$, i.e., the two components are immiscible. For small κ, the system exhibits the radial phase separation where one component is surrounded by the other one as shown in Fig. 1(a) for $\kappa = 0.75$. If the SOC is absent and the ratio $\int|\psi_\uparrow|^2 d\mathbf{r}/\int|\psi_\downarrow|^2 d\mathbf{r}$ is not fixed, the ground state is occupied only by one component for the immiscible case. The two thin rings of $n_\downarrow$ in Fig. 1(a) are therefore the effect of the SOC. With an increase in the SOC, our numerical results show that the rotational symmetry is broken and the system always shows a modified stripe phase, which is similar to that predicted for homogeneous condensates [20,22]. However, this phase is different from the previous stripe phase in that the stripe is bent near the central hole and tends to be perpendicular to the perimeter of the central hole as shown in Fig. 1(b). We note that for fixed SOC, this tendency becomes more significant as the size of the central hole is increased, which can be seen from Fig. 1(b-1) to Fig. 1(b-2).

In the limit of a very tight and narrow annulus, the system can be regarded as a quasi-1D ring. In this case, all the stripes are perpendicular to the perimeter of the central hole. The ground-state density distribution of the system therefore shows an alternately arranged stripe pattern along the ring as shown in Fig. 1(b-3). The number of stripes increases with the strength of the SOC.

More insights can be obtained if we look at the momentum-space density distributions presented in the third column of Figs. 1(a) and 1(b) where the dashed circles indicate $|\mathbf{k}| = \kappa$. For the modified stripe phases shown in Fig. 1(b), more and more $\mathbf{k}$'s around the Rashba ring are entering the condensate wave function with increasing l. In the limit of the quasi-1D ring shown in Fig. 1(b-3), $\mathbf{k}$'s with the same amplitude but different angles are uniformly distributed around the ring,

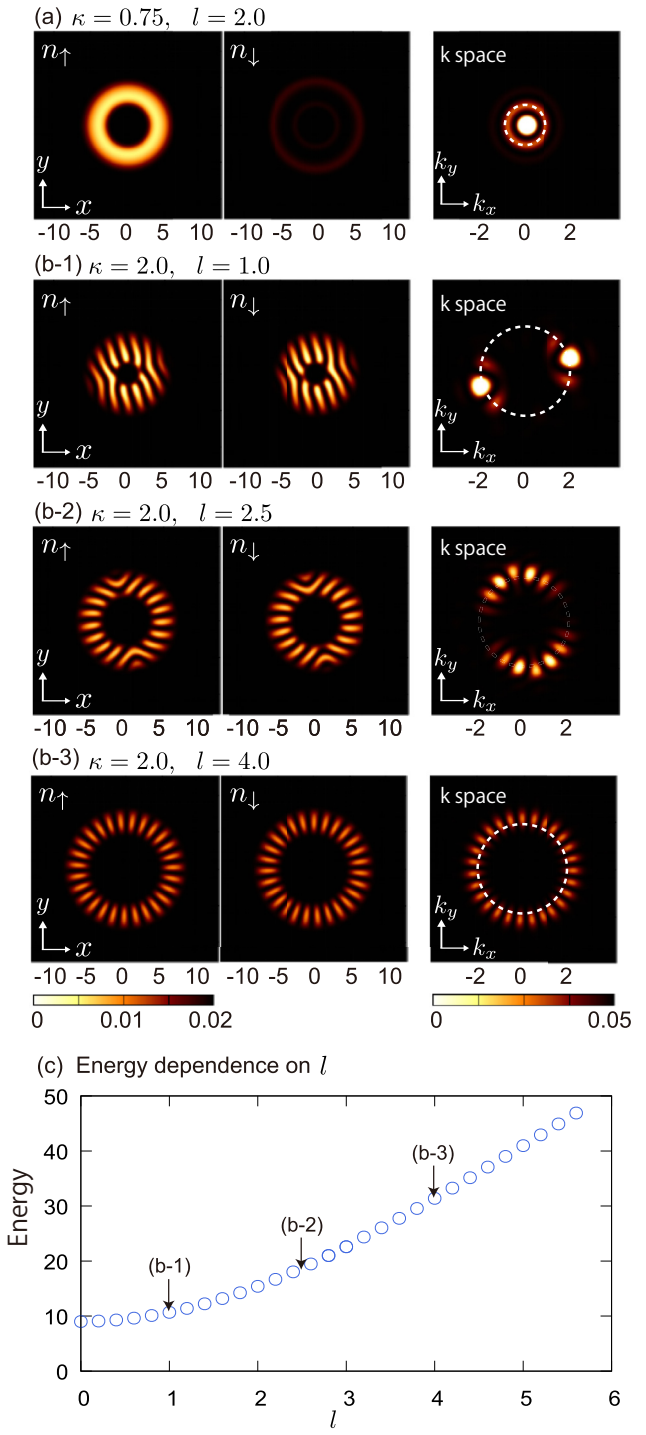

FIG. 1. Ground states in a toroidal trap for the immiscible case with $A = 100$, $g = 800$, and $g_{\uparrow\downarrow} = 1000$. (a) and (b) Density profiles of up- and down-components $n_\uparrow = |\psi_\uparrow|^2$ and $n_\downarrow = |\psi_\downarrow|^2$ and $\mathbf{k}$-space densities $\sum_{j=\uparrow,\downarrow}|\int\psi_j\exp(-i\boldsymbol{k}\cdot\boldsymbol{r})d\boldsymbol{r}|^2$ for (a) $\kappa = 0.75$ and $l = 2.0$ and (b-1)–(b-3) $\kappa = 2.0$ and $l = 1.0$, $l = 2.5$, and $l = 4.0$. The dashed circles in the $\mathbf{k}$ space indicate $|\mathbf{k}| = \kappa$. (c) Dependence of the total energy on the width l of the toroidal trap for fixed SOC $\kappa = 2.0$. The stripe state (b-1) is smoothly changed to state (b-3) as l is increased.

leading to the formation of the azimuthal stripe pattern. In Fig. 1(c), we plot the dependence of the total energy on the width l of the toroidal trap for fixed SOC $\kappa = 2.0$. We find that the stripes are changing smoothly from being vertical [Fig. 1(b-1)] to being azimuthal [Fig. 1(b-3)], which clarifies that the transition is not discrete but continuous.

Figure 2 shows the miscible cases with $g > g_{\uparrow\downarrow}$. When the central hole is small, the ground state is similar to the plane wave [20] where all the bosons are condensed into a single plane-wave state and the direction of the plane wave is chosen on the x-y plane breaking the rotational symmetry. As the central hole is increased, the effect of the toroidal potential emerges. The direction of the flow tends to be azimuthal, and the flow pattern becomes countercircling as shown in the phase distributions of Figs. 2(a-1) and 2(a-2) for $l = 1.0$ and 3.0, respectively. In this case, we observe a countercircling gradient of the wave-function phase with the rotational symmetry broken, which is visible in the density distribution. We notice that for a Rashba SO-coupled system, the actual particle current consists of both the canonical part related to the superfluid velocity and the gauge part induced by the SOC. For the countercircling flow, these two parts have the same magnitude but opposite directions. Consequently, the total particle current is zero, and no particle flows out of the potential.

For a larger l (close to the ring limit), the tendency of azimuthal flowing becomes more significant. In this case, the flow becomes one-way circulating with the rotational symmetry, and the density distribution has rotational symmetry as shown in Fig. 2(a-3) for $l = 5.0$. Meanwhile, it is well known that for a Rashba SO-coupled system, there always exists a small spatial displacement along the perpendicular direction of the phase gradient in the miscible region, which results from the spin-dependent force induced by SOC [24,47]. The spin-up component always shifts inwards all around the ring, leading to the pattern formation of density difference shown in Fig. 3(a). The above-mentioned countercircling and one-way flows can also be explained by the different momentum-space density distributions shown in the middle column of Fig. 2(a). In Fig. 2(b), we plot the dependence of the total energy on the width l for two such different structures and compare their energy difference. We find that the former (latter) state is the ground state for $l \lesssim (\gtrsim) 4.8$. Thus, the transition of the ground state among the states in Figs. 2(a-1)–2(a-3) is discrete, unlike the continuous transition in the immiscible case in Fig. 1.

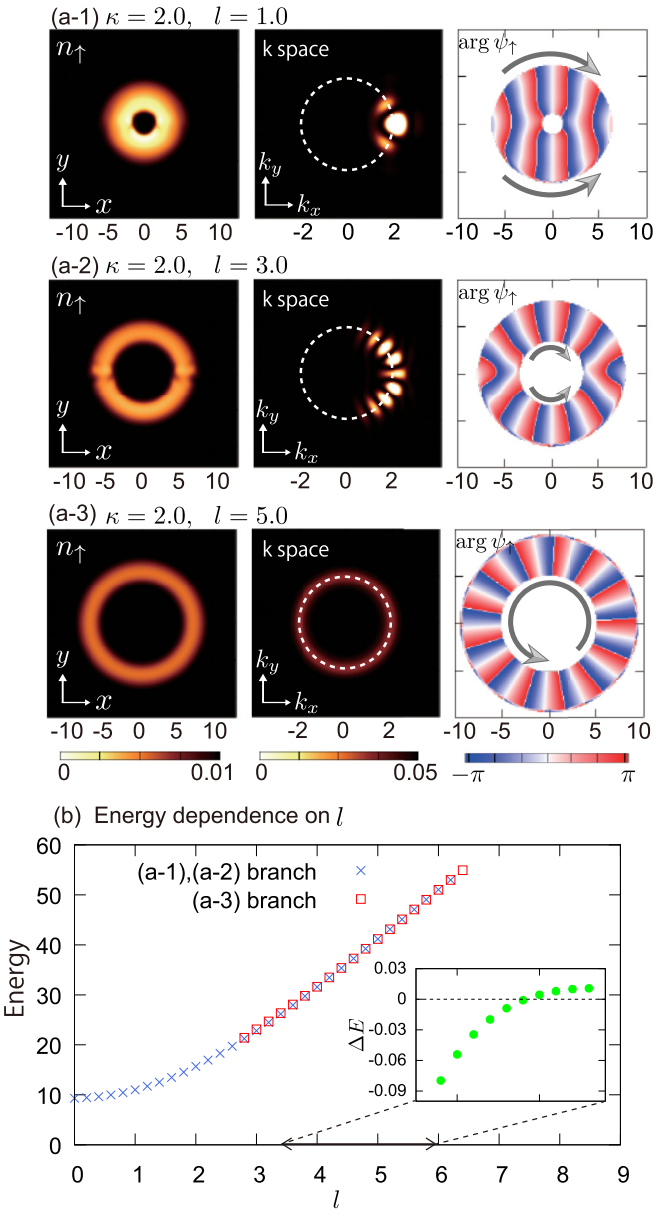

FIG. 2. Ground states in a toroidal trap for the miscible case with $A = 100$, $g = 1000$, $g_{\uparrow\downarrow} = 800$, and $\kappa = 2$. (a) Density $n_\uparrow$, **k**-space density, and phase arg $\psi_\uparrow$ distributions for $\kappa = 2.0$ and for $l = 1.0$,3.0, and 5.0, corresponding to (a-1)–(a-3), respectively. The dashed circles in the **k** space indicate $|\boldsymbol{k}| = \kappa$. In the phase distribution, the region satisfying $n_\uparrow + n_\downarrow > 10^{-4}$ is extracted, and the arrows represent the directions of the phase gradient. (b) Dependence of the total energy on the width l for two different flow structures (a-1)–(a-3). The inset shows the energy difference between two such structures within the region marked by the double-headed arrow, which indicates that the former (latter) state is the ground state for $l \lesssim (\gtrsim) 4.8$.

B. Variational analysis

The results in Figs. 1 and 2 indicate that the direction of the wave-number vector tends to be azimuthal in a toroidal trap, and this tendency is more significant for a tighter toroidal confinement. To understand this result, we employ the Gaussian variational method. For simplicity, we assume a potential $V = x^2/2$ and show that the wave-number vector becomes perpendicular to the confinement, i.e., in the y direction. For the miscible case, as we discussed before, there always exists a small spatial displacement in such two components as shown in Fig. 3(a) for the ring limit case. Thus, the variational wave functions are assumed to be

$$\psi_\uparrow = \frac{1}{\sqrt{2}} \frac{1}{\pi^{1/4}\sigma^{1/2}} e^{-[(x+X)^2/2\sigma^2]} e^{i\mathbf{k}\cdot\mathbf{r}},$$
$$\psi_\downarrow = \frac{1}{\sqrt{2}} \frac{-e^{i\phi_\mathbf{k}}}{\pi^{1/4}\sigma^{1/2}} e^{-[(x-X)^2/2\sigma^2]} e^{i\mathbf{k}\cdot\mathbf{r}}, \quad (5)$$

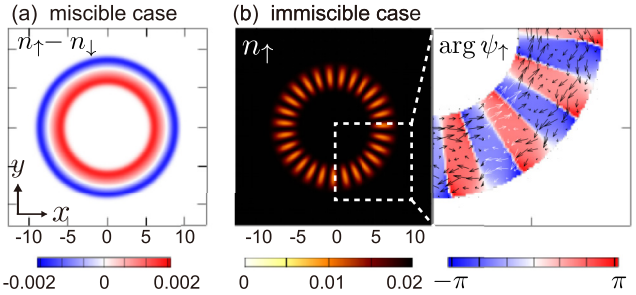

FIG. 3. (a) Density difference $n_\uparrow - n_\downarrow$ of the state in Fig. 2(a-3). (b) Density $n_\uparrow$ and phase $\arg\psi_\uparrow$ of the state in Fig. 1(b-3) where the dashed square region in the left panel is magnified in the right panel. The arrows indicate the phase gradient $(\psi_\uparrow^*\nabla\psi_\uparrow - \psi_\uparrow\nabla\psi_\uparrow^*)/(2i)$. (a) and (b) justify the variational wave functions of Eqs. (5) and (7), respectively.

where σ, X, and $\mathbf{k}$ are variational parameters and $\phi_\mathbf{k}$ is the angle between $\mathbf{k}$ and the x axis. The shift X in Eq. (5) is justified by the numerical result shown in Fig. 3(a), where $|\psi_\uparrow|^2$ and $|\psi_\downarrow|^2$ are shifted in the opposite directions perpendicular to the direction of confinement. Substituting Eq. (5) into the GP energy functional, we obtain the variational energy as

$$E = \frac{1}{4\sigma^2} + \frac{k^2}{2} + \frac{\sigma^2}{4} + \frac{X^2}{2} - \kappa\left(k + \frac{k_y}{k}\frac{X}{\sigma^2}\right)e^{-(X^2/\sigma^2)} + \frac{1}{4\sqrt{2\pi}\sigma}(g + g_{\uparrow\downarrow}e^{-(X^2/\sigma^2)}). \tag{6}$$

We note that this energy is independent of the direction of $\mathbf{k}$ if $X = 0$. Assuming $X \ll \sigma$, we find that $k_x = 0$, $k_y \simeq \pm\kappa$, and $X \simeq \pm\kappa/\sigma^2$ minimize E. The energy of the state with $\mathbf{k}$ in the y direction is smaller than that with $\mathbf{k}$ in the x direction by $\simeq\kappa^2/(2\sigma_0^4)$. Thus, in the miscible case, the ground state tends to have momentum perpendicular to the direction of confinement.

For the immiscible case, we assume that the $+\mathbf{k}$ and $-\mathbf{k}$ components shift in opposite directions of confinement. This is justified from the phase distribution in Fig. 3(b) in which the phase gradient in opposite directions emerges on the edges of the condensate. Thus, the variational wave functions can be assumed to be

$$\psi_\uparrow = \frac{1}{2\pi^{1/4}\sigma^{1/2}}[e^{-[(x-X)^2/2\sigma^2]}e^{i\mathbf{k}\cdot\mathbf{r}} + e^{-[(x+X)^2/2\sigma^2]}e^{-i\mathbf{k}\cdot\mathbf{r}}],$$
$$\psi_\downarrow = \frac{-e^{i\phi_\mathbf{k}}}{2\pi^{1/4}\sigma^{1/2}}[e^{-[(x+X)^2/2\sigma^2]}e^{i\mathbf{k}\cdot\mathbf{r}} - e^{-[(x-X)^2/2\sigma^2]}e^{-i\mathbf{k}\cdot\mathbf{r}}], \tag{7}$$

which reduces to the usual stripe state for $X = 0$. With the same procedure as above (see the Appendix), we find that the energy is minimized by $k_x = 0$, $k_y \simeq \pm\kappa$, and $X \simeq \pm\kappa/\sigma^2$, which are the same as in the miscible case. Thus, in both miscible and immiscible cases, the direction of the wave-number vector $\mathbf{k}$ tends to be perpendicular to the direction of confinement, which explains the behaviors in Figs. 1 and 2, i.e., the wave-number vector tends to be azimuthal in a toroidal trap.

IV. QUANTUM MANY-BODY ANALYSIS

We have so far considered a quasi-2D system within the mean-field approximation. When the toroidal potential is so tight that $\hbar\omega_0$ is much larger than any other energy scales and $a_0 \equiv \sqrt{\hbar/(M\omega_0)} \ll R$, the system reduces to a quasi-1D ring. In this limit, the spatial degrees of freedom are reduced, and the problem is simplified, which enables us to go beyond the mean-field approximation. For this purpose, we formulate the system of bosons with the SOC confined in a quasi-1D ring potential.

First we eliminate the radial degree of freedom in Eq. (1) and reduce the Hamiltonian to 1D. The radial wave function can be approximated by the ground state of

$$\left[-\frac{1}{2}\left(\frac{\partial^2}{\partial r^2} + \frac{1}{r}\frac{\partial}{\partial r}\right) + V_r(r)\right]f(r) = E_0 f(r), \tag{8}$$

where $\int_0^\infty f^2(r) r\,dr = 1$. Using the fact that the atoms are confined to $r \simeq R$, one can show $\int_0^\infty f^2(r)dr \simeq 1/R$ and $\int_0^\infty f(r)f'(r)r\,dr \simeq -1/(2R)$, giving

$$-i\int_0^\infty f(r)\left(\frac{\partial}{\partial x} \pm i\frac{\partial}{\partial y}\right)f(r)r\,dr \simeq \frac{ie^{\pm i\theta}}{R}\left(\frac{1}{2} \mp i\frac{\partial}{\partial\theta}\right). \tag{9}$$

Dividing the field operator into the radial and azimuthal parts as $\hat\psi_{\uparrow,\downarrow}(\mathbf{r}) = f(r)\hat\phi_{\uparrow,\downarrow}(\theta)$ and using Eq. (9), the Hamiltonian in Eq. (1) reduces to [48]

$$\hat{\mathcal{H}} = \int_0^{2\pi} d\theta\left\{\hat{\boldsymbol{\phi}}^\dagger\left(E_0 - \frac{1}{2R^2}\frac{\partial^2}{\partial\theta^2}\right)\hat{\boldsymbol{\phi}} + \frac{i\kappa}{R}\left[e^{-i\theta}\hat\phi_\uparrow^\dagger\left(\frac{1}{2} + i\frac{\partial}{\partial\theta}\right)\hat\phi_\downarrow + e^{i\theta}\hat\phi_\downarrow^\dagger\left(\frac{1}{2} - i\frac{\partial}{\partial\theta}\right)\hat\phi_\uparrow\right] + \frac{gC}{2}(\hat\phi_\uparrow^{\dagger 2}\hat\phi_\uparrow^2 + \hat\phi_\downarrow^{\dagger 2}\hat\phi_\downarrow^2) + g_{\uparrow\downarrow}C\hat\phi_\uparrow^\dagger\hat\phi_\downarrow^\dagger\hat\phi_\downarrow\hat\phi_\uparrow\right\}, \tag{10}$$

where $\hat{\boldsymbol{\phi}} = (\hat\phi_\uparrow, \hat\phi_\downarrow)^T$ and $C = \int_0^\infty f^4(r) r\,dr$. Since the total number of atoms is fixed, we neglect the term of E_0 in the following.

We expand the field operator as

$$\hat\phi_{\uparrow,\downarrow}(\theta) = \sum_{n=-\infty}^{\infty}\hat a_{\uparrow,\downarrow n}\frac{e^{in\theta}}{\sqrt{2\pi}}, \tag{11}$$

where $\hat a_{\uparrow,\downarrow n}$ satisfies the bosonic commutation relations. Substituting Eq. (11) into the one-body part of Eq. (10), we obtain

$$\hat{\mathcal{H}}_0 = \sum_{n=-\infty}^{\infty}\left[\frac{n^2}{2R^2}(\hat a_{\uparrow n}^\dagger\hat a_{\uparrow n} + \hat a_{\downarrow n}^\dagger\hat a_{\downarrow n}) + \frac{i\kappa}{R}m(\hat a_{\downarrow n+1}^\dagger\hat a_{\uparrow n} - \hat a_{\uparrow n}^\dagger\hat a_{\downarrow n+1})\right], \tag{12}$$

where $m = n + 1/2$. The second line of Eq. (12) originates from the SOC term where the strength of the coupling $\kappa m/R$ between up- and down-components is proportional to the azimuthal quantum number n. This is different from the case of Raman coupling between two components using Gaussian and Laguerre-Gaussian beams [17,38,41,49].

Using linear transformation as

$$\hat{\alpha}_m^- = \hat{a}_{\uparrow n}\cos\alpha + i\hat{a}_{\downarrow n+1}\sin\alpha,$$
$$\hat{\alpha}_m^+ = \hat{a}_{\uparrow n}\sin\alpha - i\hat{a}_{\downarrow n+1}\cos\alpha, \tag{13}$$

with $\tan 2\alpha = 2\kappa R$, Eq. (12) is diagonalized as

$$\hat{\mathcal{H}}_0 = \sum_{m=-\infty}^{\infty}(E_m^+\hat{\alpha}_m^{+\dagger}\hat{\alpha}_m^+ + E_m^-\hat{\alpha}_m^{-\dagger}\hat{\alpha}_m^-), \tag{14}$$

where

$$E_m^\pm = \frac{1}{2R^2}\left(m^2 + \frac{1}{4} \pm m\cos 2\alpha\right) \pm \frac{\kappa}{R}m\sin 2\alpha. \tag{15}$$

These energies are twofold degenerate because of $E_m^- = E_{-m}^+$. For $\kappa \gg R^{-1}$, the mixing angle becomes $\alpha \to \pi/4$, and the quasiparticles in Eq. (13) consist of the up- and down- components with equal weight where the energies are $E_m^\pm \simeq (m^2+1/4)/(2R^2) \pm \kappa m/R$. For $\kappa = 0$, the energies in Eq. (15) reduce to those of free particles in a ring $E_m^+ = (n+1)^2/(2R^2)$ and $E_m^- = n^2/(2R^2)$.

We consider the quantum many-body state that minimizes $\langle\hat{\mathcal{H}}_0\rangle$. The solution of $\partial E_m^\pm/\partial m = 0$ is given by $m = \mp\sqrt{1+(2\kappa R)^2}/2$. Let $\mp m_0$ be the half integers that are closest to $\mp\sqrt{1+(2\kappa R)^2}/2$ and minimize $E_m^\pm$, which we define as $E_{\min} = E_{\mp m_0}^\pm$. For $\kappa \gg R^{-1}$, the energy is minimized by $m_0 \simeq \kappa R$. In this case, the energy is $E_{\min} \simeq -\kappa^2/2$, and the wave number along the ring is $\simeq m_0/R \simeq \kappa$, which agree with those of the ground state for a uniform system. The N-particle states that minimize $\langle\hat{\mathcal{H}}_0\rangle$ are given by

$$|N-p,p\rangle = \frac{(\hat{\alpha}_{-m_0}^{+\dagger})^{N-p}(\hat{\alpha}_{m_0}^{-\dagger})^p}{\sqrt{(N-p)!\sqrt{p!}}}|0\rangle, \tag{16}$$

where $p = 0,1,\ldots,N$. These states satisfy $\hat{\mathcal{H}}_0|N-p,p\rangle = NE_{\min}|N-p,p\rangle$ and hence are $(N+1)$-fold degenerate. When $\kappa R < \sqrt{3}/2$, we find $\alpha < \pi/6$, $m_0 = 1/2$, and $n = 0$, and the trivial state in which all the atoms are at rest is recovered. We therefore consider the case of $\kappa R > \sqrt{3}/2$ in the following.

Next we examine the interaction energy. We assume that the ground state is spanned by the states in Eq. (16). The expectation value of the interaction part of Eq. (10) with respect to the many-body state in Eq. (16) is calculated to be

$$\langle N-p,p|\hat{\mathcal{H}}_{\rm int}|N-p,p\rangle$$
$$= \frac{C}{16\pi}[3g + g_{\uparrow\downarrow} + (g-g_{\uparrow\downarrow})\cos 4\alpha]N(N-1)$$
$$- \frac{C}{8\pi}(g-g_{\uparrow\downarrow})(1+3\cos 4\alpha)p(N-p). \tag{17}$$

The matrix element $\langle N-p,p|\hat{\mathcal{H}}_{\rm int}|N-p',p'\rangle$ vanishes for $p \neq p'$. The first term on the right-hand side of Eq. (17) is constant and unimportant. In the second term, $1+3\cos 4\alpha$ is negative since we are considering the case of $\pi/6 < \alpha < \pi/4$. Therefore, the interaction energy is minimized by $p = 0$ or $p = N$ for $g > g_{\uparrow\downarrow}$, i.e., the many-body ground state is $|N,0\rangle$ or $|0,N\rangle$. These states correspond to the plane-wave state since all the atoms have the same momentum along the quasi-1D ring.

For $g < g_{\uparrow\downarrow}$, the interaction energy in Eq. (17) is minimized by $p = N/2$, i.e., the ground state is $|N/2,N/2\rangle$, which is the fragmented BEC [14,50,51]. This state has rotational symmetry about the z axis reflecting the symmetry of the Hamiltonian. However, if we measure the density distribution of this state, alternate domains of the two components are observed, which correspond to the stripe phase in the mean-field theory. This is understood from the density correlations of state $|N/2,N/2\rangle$,

$$\langle\hat{\phi}_\uparrow^\dagger(\theta)\hat{\phi}_\uparrow^\dagger(\theta+\Delta\theta)\hat{\phi}_\uparrow(\theta+\Delta\theta)\hat{\phi}_\uparrow(\theta)\rangle$$
$$= \langle\hat{\phi}_\downarrow^\dagger(\theta)\hat{\phi}_\downarrow^\dagger(\theta+\Delta\theta)\hat{\phi}_\downarrow(\theta+\Delta\theta)\hat{\phi}_\downarrow(\theta)\rangle$$
$$= \frac{N}{16\pi^2}\left[N - 1 - \cos^2 2\alpha + \frac{N}{2}\sin^2 2\alpha\,\cos(2m_0\Delta\theta)\right], \tag{18}$$

$$\langle\hat{\phi}_\uparrow^\dagger(\theta)\hat{\phi}_\downarrow^\dagger(\theta+\Delta\theta)\hat{\phi}_\downarrow(\theta+\Delta\theta)\hat{\phi}_\uparrow(\theta)\rangle$$
$$= \frac{N}{16\pi^2}\left[N - \sin^2 2\alpha - \frac{N}{2}\sin^2 2\alpha\,\cos(2m_0\Delta\theta)\right]. \tag{19}$$

These correlation functions indicate that, if an up-component atom is detected at θ, a down-component atom is more likely to be detected at $\theta + \nu\pi/(2m_0)$ than another up-component atom, where ν is an integer [52]. Thus, the fragmented state $|N/2,N/2\rangle$ corresponds to the stripe along the ring with a wavelength of $2m_0$.

The approximation that the ground state is spanned only by the states in Eq. (16) is valid when the interaction energy $g\rho$ is much smaller than the azimuthal kinetic-energy $\hbar^2/(MR^2)$ and the SOC energy $\hbar^2\kappa^2/M$, where $\rho = N/(Ra_0a_z)$ is the typical density. These conditions are rewritten as $NaR/(a_0a_z) \ll 1$ and $Na/(\kappa a_0a_z) \ll 1$ and are satisfied by, e.g., $N \sim 100$, $a \sim 0.1$ nm, $R \sim 10$, $a_0 \sim a_z \sim 1$ μm, and $\kappa \gg R^{-1}$, which can be realized by Feshbach resonance. These conditions are relaxed if we allow excitations above the many-body state in Eq. (16). In such a case, multiple azimuthal angular momenta m must be taken into account, and the numerical diagonalization is needed to obtain the ground state [45].

V. CONCLUSIONS

We have investigated the effect of a toroidal trap on SO-coupled BECs. In contrast to the case of the harmonic trap, the interplay between the SOC and the toroidal trap can result in a rich variety of ground states, such as a modified stripe, an alternately arranged stripe, and countercircling states. We found that the condensate in a toroidal trap tends to have wave-number vectors in the azimuthal direction, which becomes more significant for a tighter toroidal trap. This finding can be explained by the Gaussian variational analysis. We also have formulated a quantum many-body problem for the quasi-1D ring trap for both miscible and immiscible cases. In the latter case, the ground state of the system is found to be a fragmented condensate. Owing to the recent developments in the experimental implementation of SOC and the high degrees of control over most of the system parameters, the various states found in this paper may be observed in current experiments.

ACKNOWLEDGMENTS

This work was supported by JSPS KAKENHI Grants No. JP16K05505, No. JP26400414, and No. JP25103007, by the NSFC under Grants No. 61127901 and No. 11547126, and by the Youth Innovation Promotion Association of CAS under Grant No. 2015334.

X.-F.Z. and M.K. contributed equally to this work.

APPENDIX: VARIATIONAL ANALYSIS IN THE IMMISCIBLE CASE

Substituting Eq. (7) into the GP energy functional and integrating with respect to x, we obtain

$$E_{\text{kinetic}} = \frac{1}{4\sigma^2} + \frac{k^2}{2}, \tag{A1}$$

$$E_{\text{potential}} = \frac{\sigma^2}{4} + \frac{X^2}{2}, \tag{A2}$$

$$E_{\text{soc}} = -\kappa\left(k + \frac{k_y}{k}\frac{X}{\sigma^2}\right)e^{-[X^2/\sigma^2]} + ie^{-k_x^2\sigma^2}k_y\cos(2k_xX+\theta)\cos 2k_y y, \tag{A3}$$

$$E_{\text{interaction}} = \frac{1}{8\sqrt{2\pi}\sigma}[g(1+2e^{-[2X^2/\sigma^2]}) + g_{\uparrow\downarrow} - (g_{\uparrow\downarrow}-g)e^{-2k_x^2\sigma^2-[2X^2/\sigma^2]}\cos 4k_y y], \tag{A4}$$

where E_{kinetic} and $E_{\text{potential}}$ are the same as those in the miscible case in Eq. (6). The second line of Eq. (A3) vanishes by integrating with respect to y. Similarly, the second line of Eq. (A4) also vanishes for $k_y \neq 0$. In this case, assuming $X \ll \sigma$, one finds that $k_x = 0$, $k_y \simeq \pm\kappa$, and $X \simeq \pm\kappa/\sigma^2$ minimize the total energy. The energy lowered by the shift X is $\simeq\kappa^2/(2\sigma^4)$. When the immiscible interaction energy dominates the SOC energy, the second line of Eq. (A4) is minimized by $k_x = k_y = 0$ and $X = 0$, which corresponds to the state shown in Fig. 1(a).

[1] Y.-J. Lin, R. L. Compton, K. Jiménez-García, J. V. Porto, and I. B. Spielman, Nature (London) **462**, 628 (2009).
[2] Y.-J. Lin, R. L. Compton, A. R. Perry, W. D. Phillips, J. V. Porto, and I. B. Spielman, Phys. Rev. Lett. **102**, 130401 (2009).
[3] Y.-J. Lin, K. Jiménez-García, and I. B. Spielman, Nature (London) **471**, 83 (2011).
[4] Y.-J. Lin, R. L. Compton, K. Jiménez-García, W. D. Phillips, J. V. Porto, and I. B. Spielman, Nat. Phys. **7**, 531 (2011).
[5] P. Wang, Z.-Q. Yu, Z. Fu, J. Miao, L. Huang, S. Chai, H. Zhai, and J. Zhang, Phys. Rev. Lett. **109**, 095301 (2012).
[6] B. M. Anderson, G. Juzeliūnas, V. M. Galitski, and I. B. Spielman, Phys. Rev. Lett. **108**, 235301 (2012).
[7] Z. Fu, L. Huang, Z. Meng, P. Wang, L. Zhang, S. Zhang, H. Zhai, P. Zhang, and J. Zhang, Nat. Phys. **10**, 110 (2014).
[8] S. C. Ji, J. Y. Zhang, L. Zhang, Z. D. Du, W. Zheng, Y. J. Deng, H. Zhai, S. Chen, and J. W. Pan, Nat. Phys. **10**, 314 (2014).
[9] L. Huang, Z. Meng, P. Wang, P. Peng, S.-L. Zhang, L. Chen, D. Li, Q. Zhou, and J. Zhang, Nat. Phys. **12**, 540 (2016).
[10] Z. Wu, L. Zhang, W. Sun, X.-T. Xu, B.-Z. Wang, S.-C. Ji, Y. Deng, S. Chen, X.-J. Liu, and J.-W. Pan, Science **354**, 83 (2016).
[11] M. Z. Hasan and C. L. Kane, Rev. Mod. Phys. **82**, 3045 (2010).
[12] X.-L. Qi and S.-C. Zhang, Rev. Mod. Phys. **83**, 1057 (2011).
[13] J. Dalibard, F. Gerbier, Juzeliūnas, and P. Öhberg, Rev. Mod. Phys. **83**, 1523 (2011).
[14] C. J. Wu, I. Mondragon-Shem, and X. F. Zhou, Chin. Phys. Lett. **28**, 097102 (2011).
[15] N. Goldman, G. Juzeliūnas, P. Öhberg, and I. B. Spielman, Rep. Prog. Phys. **77**, 126401 (2014).
[16] H. Zhai, Rep. Prog. Phys. **78**, 026001 (2015).
[17] K. Sun, C. Qu, and C. Zhang, Phys. Rev. A **91**, 063627 (2015).
[18] M. DeMarco and H. Pu, Phys. Rev. A **91**, 033630 (2015).
[19] C. Qu, K. Sun, and C. Zhang, Phys. Rev. A **91**, 053630 (2015).
[20] C. Wang, C. Gao, C.-M. Jian, and H. Zhai, Phys. Rev. Lett. **105**, 160403 (2010).
[21] T.-L. Ho and S. Zhang, Phys. Rev. Lett. **107**, 150403 (2011).
[22] S. Sinha, R. Nath, and L. Santos, Phys. Rev. Lett. **107**, 270401 (2011).
[23] H. Hu, B. Ramachandhran, H. Pu, and X.-J. Liu, Phys. Rev. Lett. **108**, 010402 (2012).
[24] Y. Zhang, L. Mao, and C. Zhang, Phys. Rev. Lett. **108**, 035302 (2012).
[25] Y. Li, L. P. Pitaevskii, and S. Stringari, Phys. Rev. Lett. **108**, 225301 (2012).
[26] T. Kawakami, T. Mizushima, M. Nitta, and K. Machida, Phys. Rev. Lett. **109**, 015301 (2012).
[27] B. Ramachandhran, B. Opanchuk, X.-J. Liu, H. Pu, P. D. Drummond, and H. Hu, Phys. Rev. A **85**, 023606 (2012).
[28] E. Ruokokoski, J. A. M. Huhtamäki, and M. Möttönen, Phys. Rev. A **86**, 051607(R) (2012).
[29] X.-Q. Xu and J. H. Han, Phys. Rev. Lett. **107**, 200401 (2011).
[30] J. Radić, T. A. Sedrakyan, I. B. Spielman, and V. Galitski, Phys. Rev. A **84**, 063604 (2011).
[31] X. F. Zhou, J. Zhou, and C. J. Wu, Phys. Rev. A **84**, 063624 (2011).
[32] A. Aftalion and P. Mason, Phys. Rev. A **88**, 023610 (2013).
[33] H. Sakaguchi and K. Umeda, J. Phys. Soc. Jpn. **85**, 064402 (2016).
[34] S. Eckel, J. G. Lee, F. Jendrzejewski, N. Murray, C. W. Clark, C. J. Lobb, W. D. Phillips, M. Edwards, and G. K. Campbell, Nature (London) **506**, 200 (2014).
[35] A. A. Wood, B. H. J. McKellar, and A. M. Martin, Phys. Rev. Lett. **116**, 250403 (2016).
[36] F. Jendrzejewski, S. Eckel, N. Murray, C. Lanier, M. Edwards, C. J. Lobb, and G. K. Campbell, Phys. Rev. Lett. **113**, 045305 (2014).
[37] L. Corman, L. Chomaz, T. Bienaimé, R. Desbuquois, C. Weitenberg, S. Nascimbéne, J. Dalibard, and J. Beugnon, Phys. Rev. Lett. **113**, 135302 (2014).
[38] S. Beattie, S. Moulder, R. J. Fletcher, and Z. Hadzibabic, Phys. Rev. Lett. **110**, 025301 (2013).

[39] K. C. Wright, R. B. Blakestad, C. J. Lobb, W. D. Phillips, and G. K. Campbell, Phys. Rev. Lett. **110**, 025302 (2013).
[40] C. Ryu, P. W. Blackburn, A. A. Blinova, and M. G. Boshier, Phys. Rev. Lett. **111**, 205301 (2013).
[41] C. Ryu, M. F. Andersen, P. Cladé, V. Natarajan, K. Helmerson, and W. D. Phillips, Phys. Rev. Lett. **99**, 260401 (2007).
[42] S. Bargi, F. Malet, G. M. Kavoulakis, and S. M. Reimann, Phys. Rev. A **82**, 043631 (2010).
[43] M. Abad, A. Sartori, S. Finazzi, and A. Recati, Phys. Rev. A **89**, 053602 (2014).
[44] A. Muñoz Mateo, A. Gallemí, M. Guilleumas, and R. Mayol, Phys. Rev. A **91**, 063625 (2015).
[45] R. Kanamoto, H. Saito, and M. Ueda, Phys. Rev. Lett. **94**, 090404 (2005).
[46] T. Shimodaira, T. Kishimoto, and H. Saito, Phys. Rev. A **82**, 013647 (2010).
[47] S.-W. Song, Y.-C. Zhang, L. Wen, and H. Wang, J. Phys. B **46**, 145304 (2013).
[48] O. Fialko, J. Brand, and U. Zülicke, Phys. Rev. A **85**, 051605(R) (2012).
[49] L. Chen, H. Pu, and Y. Zhang, Phys. Rev. A **93**, 013629 (2016).
[50] S. Gopalakrishnan, A. Lamacraft, and P. M. Goldbart, Phys. Rev. A **84**, 061604(R) (2011).
[51] S.-W. Song, Y.-C. Zhang, H. Zhao, X. Wang, and W.-M. Liu, Phys. Rev. A **89**, 063613 (2014).
[52] J. Javanainen and S. M. Yoo, Phys. Rev. Lett. **76**, 161 (1996).